2013

Sol-gel Characteristics for Corrosion Resistance of Anodised Aluminium

Michael Whelan
Technological University Dublin, michael.g.whelan@tudublin.ie

John Cassidy
Technological University Dublin, john.cassidy@tudublin.ie

Brendan Duffy
Technological University Dublin, brendan.duffy@tudublin.ie

Recommended Citation

Whelan, M., Cassidy, J., Duffy, B.: (2013) Solar gel sealing characteristics for corrosion resistance of anodised aluminium. *Surface and Coatings Technology,* Volume 235, 25 November 2013, pp. 86-96, ISSN 0257-8972, doi:10.1016/j.surfcoat.2013.07.018 Available from the publisher here

Surface & Coatings Technology 235 (2013) 86–96

Contents lists available at ScienceDirect

Surface & Coatings Technology

journal homepage: www.elsevier.com/locate/surfcoat

Sol–gel sealing characteristics for corrosion resistance of anodised aluminium

M. Whelan [a,*], J. Cassidy [b], B. Duffy [a]

[a] Centre for Research in Engineering Surface Technology, Focas Institute, Dublin Institute of Technology, Kevin St, Dublin 8, Ireland
[b] Department of Chemical and Pharmaceutical Science, Dublin Institute of Technology, Kevin St, Dublin 8, Ireland

ARTICLE INFO

Article history:
Received 21 November 2012
Accepted in revised form 6 July 2013
Available online 13 July 2013

Keywords:
Anodised
Sol–gel
Sealing
Corrosion

ABSTRACT

Conventional anodising electrolytes based on sulphuric acid, oxalic acid and phosphoric acid have been used to form nanoporous layers on AA3003-H14 and sealed with silane based sol–gel sealers. It is shown that the sol–gel chemistries have varying levels of pore penetration depending on the synthesis conditions. The extent of sol–gel penetration and pore sealing is analysed by electron microscopy and energy dispersive X-ray spectroscopy. To describe the sealing phenomena observed a sol–gel penetration and sealing rating has been proposed to explain the interactions of the sol–gels with the pores of the anodised layers. The corrosion resistance of the sol–gel sealed anodised aluminium surfaces was evaluated using neutral salt spray testing and electrochemical impedance spectroscopy.

1. Introduction

Aluminium is used extensively for lightweight structures such as automotive and aerospace components where the combination of strength and corrosion resistance is essential. Aluminium owes its inherent corrosion resistance to a naturally occurring passive oxide which forms on the metal when exposed to the atmosphere [1]. This oxide has a nanoscale thickness which limits the metals performance against extreme mechanical and chemical attacks [2].

Anodising is a process which increases the thickness of the aluminium oxide through an electrochemical reaction in acidic electrolytes such as sulphuric, phosphoric or oxalic acids. The features and properties of the anodic oxides produced are dependent on many parameters including the aluminium alloy used, electrolyte type and anodising conditions (e.g. temperature and current density). The process is commonly used to increase corrosion resistance and adhesion properties of the aluminium surface for a variety of applications.

The anodised aluminium oxide layer is nanoporous in structure with a self assembled, hexagonal array of pores extending from the surface of the oxide to a thin barrier layer at the metal oxide interface. The oxide growth and nanopore formation mechanism has been recently proven to result from a flow of anodic alumina in the barrier layer region due to the combination of growth stresses and field assisted plasticity [3–5]. The stresses that drive the flow of material are due to electrostriction of the oxide layer which is plasticised under the electric field [4–6]. The flow of material proceeds from the barrier layer into the pore walls forming Al_2O_3 columns in a self assembled structure.

In order to fully protect the underlying aluminium metal the porous oxide layer requires a sealing treatment to prevent penetration of aggressive corrosion inducing ions or chemicals to the base metal. Historically the most effective sealing has been achieved using Cr^{6+} compounds which impart excellent corrosion resistance to the metal due to the self healing ability of the Cr^{6+} ions [7]. These compounds however are known carcinogens and restrictions are enforced in many industries forcing alternative chemistries to be adopted [8]. A recent review of sealing processes benchmarked replacement sealing technologies for sodium dichromate sealing such as hydrothermal, sodium silicate and nickel based sealers [9]. The sealing mechanisms reviewed include chemically altering the surface of the anodised layers to close the pores by forming aluminium hydroxide, alumino-silicates or nickel hydroxides to block the pore mouths. Though these sealers have been shown to be promising replacements for Cr based sealers some concerns still exist regarding high production costs, long term exposure performance and environmental issues.

Sol–gel materials have been extensively studied for corrosion control replacements for Cr(VI) based conversion coatings. The sol–gel process can be used to form nanostructured inorganic films (typically 200 nm to 10 μm in overall thickness) that can be tailored to be more resistant than metals to oxidation, corrosion, erosion and wear while also possessing good thermal and electrical properties [10–12]. The chemistry of the sol–gel process is well known [13–16] with excellent reviews [17–19] and books [20] available. The most common sol–gel materials used as coatings are based on organically modified silicates (ormosils), which are formed by the hydrolysis and condensation of alkoxide precursors [21].

* Corresponding author. Tel.: +353 402 7968; fax: +353 402 7941.
E-mail address: michael.g.whelan@dit.ie (M. Whelan).

0257-8972/$ – see front matter
http://dx.doi.org/10.1016/j.surfcoat.2013.07.018

Despite the breadth of research conducted in the area of sol–gel corrosion control, little research has been published in the use of sol–gel sealing of anodised layers to enhance corrosion resistance. A previous study reported that zirconium oxide sol–gel films dip coated on phosphoric acid anodised aluminium films enhanced alkaline corrosion resistance [22]. The sols were applied by several dip coating cycles and the use of a boiling water treatment increased the alkaline resistance of the surfaces. The results suggested that some reaction by products of the boiling water treatment in the coating layer enhances the corrosion resistance. Subsequent research found that UV irradiation curing of the sol–gel produced a further improvement in alkaline corrosion resistant compared to thermally cured coatings [23]. A PTFE/silane system for anodised aluminium substrates with SiO_2/TiO_2 nano-fillers and a dispersion of various PTFE based fillers has also been reported [24]. The system combined the non-stick, low surface energy properties of PTFE with high scratch resistance and durability of the silane sol–gel. Vacuum dip coating of a TiO_2 based sol–gel coating was also conducted on oxalic acid anodised aluminium substrates [25]. It was shown that due to the air pressure inside the porous alumina the TiO_2 colloidal solution cannot penetrate the pores and vacuum dip coating is required to dispel the air pressure. Interestingly the authors showed that the addition of the crystalline anatase form of TiO_2 inside the pores of the anodised layers effectively inhibits the corrosion of the aluminium substrate when compared to unsealed anodised films.

It is unlikely that there is any chemical change in the bulk anodised aluminium layers due to sol–gel deposition, if the process is carried out at temperatures below 80° (temperature for boehmite conversion [1]). The penetration of sol–gel material in porous anodised structures may be considered to be key to obtaining corrosion resistance comparable to existing commercially used mechanisms. Current studies provide little evidence that sol–gel materials can be fully incorporated into anodised layers for corrosion protection, and findings to date have utilised the assistance of a vacuum deposition technique [25] or an electromotive force [26,27] to influence sol–gel impregnation. It has been reported that the charge on the surface of the anodic layers can play a role in the possible penetration of silica particles in the pores of anodic alumina [28] though current literature provides little clarification on the important parameters required for pore penetration of sol–gel materials, in anodic films, for corrosion control.

This study will analyse the interactions between silane based sol–gel chemistries and anodised layers including the pore penetration and compare corrosion performance on different anodised aluminium layers. Sol–gel films based on Tetraethylorthosilicate (TEOS) and Phenyltriethoxysilane (PhTEOS) have been used as sealing chemistries for anodic layers formed in sulphuric, oxalic and phosphoric acid electrolytes. The effect of pore sizes produced from each electrolyte on the sol–gel penetration has been investigated by FESEM and EDX. Sol–gel sealers prepared by both acid and base hydrolysis have been used to determine the effect of pH on penetration of sol–gel in the pores of the anodic layers. Corrosion evaluation has been conducted using neutral salt spray testing and electrochemical impedance spectroscopy.

2. Experimental

2.1. Sol–gel preparation

The silane precursors Tetraethylorthosilicate (TEOS) (98%) and Phenyltriethoxysilane (PhTEOS) (98%) were purchased from VWR International Ltd. (Irl), and hydrolysed separately under both acidic and alkaline conditions using 0.04 M HNO_3 and 0.1 M NH_4OH respectively. Absolute ethanol was immediately added to each mixture and left to stir for 45 min. De-ionised water was then added dropwise and the final solution was left to stir for 24 h before use. The final molar ratios for the acid catalysed (AC) and base catalysed (BC) formulations (silane:ethanol:water) were 1:2.5:3.5 and 1:3:4 respectively.

2.2. Particle size analysis

The particle size of the colloidal sol–gel dispersions was measured by a dynamic light scattering method using a Malvern Zetasizer ZS. Dynamic light scattering records the hydrodynamic diameter of the colloidal sol–gel particles undergoing Brownian motion in a dispersant of known viscosity and refractive index. By measuring the scattered light fluctuations with detectors at 90° or 173° from the sample the hydrodynamic diameter can be determined. The system was calibrated before analysis using a standard polystyrene latex material with particle size of 300 nm. The sol–gel was filtered though a 0.2 μm syringe filter to remove large contaminants from the sol–gel. A disposable cuvette cell was used for the measurement which was pre-cleaned using 0.2 μm filtered high purity ethanol.

2.3. Anodisation

AA3003-H14 (Si 0.6%, Fe 0.7%, Cu 0.05–0.25, Mn 1–1.15%, Zn 0.1%, other 0.15%, Al remainder) aluminium panels (150mm × 100mm × 0.6mm) were sourced from Q-Lab Europe Ltd. All pretreatment and anodising chemicals were purchased from Sigma Aldrich (IRL). The panels were degreased in acetone, etched in 10% NaOH at 40 °C for 50 s and rinsed in de-ionised water. The panels were then treated in 50% HNO_3 at room temperature for 90 s to remove any intermetallics from the surface prior to anodising. Anodising solutions were prepared using H_2SO_4 (98%), $C_2O_4H_2 \cdot 2H_2O$ and H_3PO_4 (85%) in de-ionised water. A 25% w/v and a 3% w/v solution of sulphuric acid and oxalic acid respectively were used for anodising at a constant current of 1.5 A/dm^2. For both acids the anodising times was 20 min. Phosphoric acid was prepared at 10% w/v and anodised at a constant of 40 V for 60 min. The anodising cell consisted of a counter electrode made of lead and the power was supplied by a Hewlett Packard DC power supply. Following anodisation the panels were rinsed for 20 min in an agitated de-ionised water bath to remove residual electrolyte from the pores. The panels were then force dried with hot air.

2.4. Sol–gel deposition

The aluminium oxide naturally hydrates in the atmosphere reducing the pore diameter. In the case of sulphuric and oxalic acid anodising the pores can fully close due to natural hydration. The anodic layers were therefore dip coated in the sol–gel formulations immediately after anodising, rinsing and drying using a KSV DC dip coater. The dip cycle consisted of a 20 minute immersion step in the sol–gel solution following withdrawal at a rate of 10 $mm.min^{-1}$. The panels were then cured in an oven at 110 °C for 16 h. The three anodic finishes were dip coated in the four formulations (AC TEOS, BC TEOS, AC PhTEOS and BC PhTEOS). Unsealed anodised panels were used as reference controls and were left unexposed for 1 week prior to testing.

2.5. Electron microscopy characterization and rating

The pore dimensions and penetration of the sol–gel sealers into the anodic layers were determined by electron microscopy using a Hitachi SU 70 Field Emission Scanning Electron Microscope (FESEM). Anodic film cross sections were prepared by bending the aluminium sample over 180° to induce micro-cracks in the oxide layer. The cross section of the crack face exhibits the pore structure of the anodic alumina for imaging at 1.5–3 keV. For imaging purposes the samples were sputter coated with a 4 nm layer of Pt/Pd using a Cressington 208HR sputter coater.

Dot Map energy dispersive X-ray spectroscopy was conducted using an Oxford Instruments INCA X-MAX Energy Dispersive X-ray Spectrometer. Cross sections were prepared by mounting samples in an epoxy resin before grinding using progressive grades of carbide paper and polished to a mirror finish with diamond solutions. The

polished cross sections were coated with 5 nm of carbon using a Cresssington 208C carbon evaporation coating unit. The Si based sol–gels can be identified by analysing the Si species overlapping with the oxide layer elements. The EDX maps are displayed as mixed maps of Al, O and Si.

A rating system was developed utilising both FESEM imaging and EDX Dot Mapping in order to grade the degree of sealing of each sol–gel on the anodic layers. The rating consists of a letter denoting the degree of penetration of sol–gel materials followed by a numerical grade of the level of pore closure. The grades are outlined in Table 1.

2.6. Accelerated corrosion testing

Corrosion resistance testing was conducted in a neutral salt spray environment according to BS EN ISO 9227:2006 with the back and sides of each panel protected with an impermeable electrically insulating tape. The test conditions consisted of a neutral salt fog atmosphere generated from 5 wt.% aqueous NaCl solution at 35 ± 1 °C. The panels were placed at an angle of 20° (±5) from the vertical to allow the salt spray to settle on the test face. The panels were exposed to the corrosive conditions for up to 2000 h. A corrosion rating was assigned after each inspection based on the grid method specified in BS EN ISO 12373-19:2001.

2.7. Electrochemical corrosion testing

Electrochemical impedance spectroscopy (EIS) was carried out using a Solartron SI 1287/1255B system comprising of a frequency analyser and potentiostat operated by CorrView® and Z Plot® software. EIS electrochemical cells were made by mounting bottom-less plastic vials on to the exposed surface of the coated panel with amine hardened (Araldite®) epoxy adhesive. The electrolyte used was a 3.5% w/v solution of NaCl(aq). The area of the coating exposed was 4.9 cm^2. The EIS analysis involved applying an AC voltage at the open circuit potential (OCP), with sinusoidal amplitude of 10 mV, from a frequency of 10^6 Hz down to 10^{-1} Hz across the anodic layers. The film resistance to the AC signal, or impedance, varies according to the applied frequency and is graphically represented on a Bode frequency plot. From this plot information can be derived relating to the electrochemical response of the anodic film to the applied potential and has been widely used as a technique to determine the physical and protective properties of anodic films [29,30]. Practical criteria have been established to assess the corrosion resistance properties of anodic layers by EIS [31]. By utilising the low frequency (0.1 Hz) impedance response a deduction can be made on the practical corrosion resistance properties of the anodic layers [31,32]. It has been proposed that if the tested system exhibits a Log |Z| value greater than 6 (impedance is greater than 10^6 Ω cm^2) after 168 h NaCl immersion the anodised metal has appropriate corrosion resistance for practical use. Furthermore by using an equivalent circuit model it is possible to separate the contributions of the porous and barrier layers as well as any contributions associated with the onset of corrosion [33]. These features are represented by individual resistances and capacitances in an appropriate equivalent circuit. The capacitors are represented as constant phase elements to account for the irregularities in the various features of the anodic layer.

Table 1
Sol gel sealing rating.

Rating	Degree of penetration	Rating	Degree of pore closure
A	Full penetration through oxide	1	Full closure
B	Partial penetration	2	Partial closure
C	Limited/no detectable penetration	3	No closure
D	Surface film only		

3. Results

3.1. Pore size

FESEM analysis of the anodic layer pore structures was used to determine the impregnation of the sol–gel colloids in the pores of the anodised layer. The three unsealed anodic finishes possessed varying pore features and dimensions as expected (Fig. 1). The SAA, OAA and PAA films possess pore diameters of 10–15 nm, 25–30 nm and 75–100 nm respectively. The SAA and OAA films produce highly ordered straight pores extending from the barrier layer to the oxide surface. In contrast the PAA films appear to contain voids in the pore channel walls connecting each adjacent pore with less interporosity near the base of the oxide layer.

3.2. Particle size

Particle size distributions of the sol–gel materials acquired by dynamic light scattering (Fig. 2) indicate that all the sol–gels contain particles sufficiently small to penetrate into the pores of the anodised layers. The sol–gels prepared show distributions as follows: AC TEOS — 4 nm to 24 nm, BC TEOS — 8 nm to 34 nm, AC PhTEOS — 3 nm to 15 nm, and BC PhTEOS — 5 nm to 17 nm. The sizes of the sol–gel colloids are particularly suitable to penetrate the OAA and PAA pores. The SAA films, with a maximum pore diameter of 15 nm, may inhibit the penetration of the larger particles of each system. The BC TEOS average particle sizes are larger than the pores of the SAA films and penetration is expected to be limited.

3.3. Pore penetration

3.3.1. Sulphuric acid anodising

The mixed elemental Dot Map for the sol–gel sealed SAA layers can be seen in Fig. 3. It is evident that for both the AC systems the presence of Si throughout the oxide is detected. From the BC TEOS system there is no detectable Si penetration into the anodic oxide which is expected due to the large particle size. There is also a detectable Si signal from the BC PhTEOS sealed SAA layer indicating penetration has occurred. In all cases there does not appear to be any significant pore closing due to the presence of the sol–gel sealers. The sol–gel penetration and pore sealing ratings for the SAA sealed anodic layers can be seen in Table 2.

From the assigned ratings it can be seen that all systems exhibited a pore closure rating of 3 as no detectable pore blocking was evident from the FESEM images. The BC TEOS system produced a D penetration rating due to the absence of a Si signal in the Dot Map and evidence of a surface film from the Dot Map and FESEM image. The AC systems and the BC PhTEOS were assigned an A penetration rating due to a significant detectable Si across the oxide layer.

3.3.2. Oxalic acid anodising

In agreement with the SAA anodic layer the AC sol–gels appear to have a higher level of penetration into the porous oxide structure when compared to the BC equivalents. The mixed elemental Dot Map (Fig. 4) shows a significant Si signal for the AC TEOS and AC PhTEOS overlapping with the oxide characteristic elements. For the AC TEOS OAA system the pathways between the surface and the base metal are closed in many areas of each pore though full closure is not achieved. Conversely the BC TEOS could not be detected within the pores by imaging and the corresponding Dot Map produced limited evidence of Si in the anodic layer. The corresponding seal ratings for the AC and BC TEOS are A2 and D3 respectively (Table 2). The AC TEOS OAA pore showed elevated closure due to the presence of the sol–gel when compared to the AC TEOS SAA (rating A3 and A2 respectively). The AC PhTEOS OAA pores achieved an A2 seal rating as they appeared closed in many areas of the FESEM image and Si could be

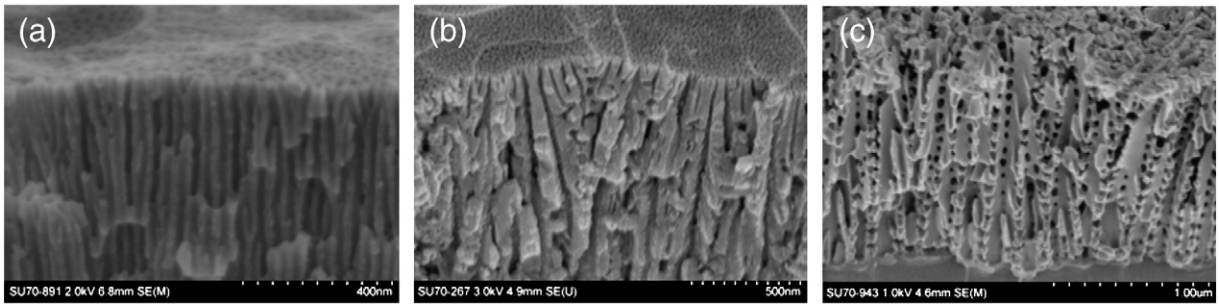

Fig. 1. FESEM micrographs of nanopores produced from (a) sulphuric acid, (b) oxalic acid and (c) phosphoric acid.

detected throughout the anodic layer. The presence of BC PhTEOS in the oxide layer was undetectable by EDX and imaging.

3.3.3. Phosphoric acid anodising

With the largest pore size and the hydration resistant properties of the anodic layer PAA offers the best opportunity of impregnation of the sol–gel materials into the porous oxide. The presence of the AC TEOS and AC PhTEOS was detected by EDX analysis, Fig. 5. In the case of AC TEOS the sol–gel preferentially accumulates at the base of the pores (Fig. 6(a)) while the AC PhTEOS sealed PAA films show a highly dense sealed oxide with sol–gel present in all areas of the anodic layer. The AC PhTEOS PAA was the only system to achieve the highest sealing grade, A1. The EDX analysis of the BC TEOS shows clearly the presence of a surface film. On closer inspection of the FESEM micrographs, a small quantity of nanoparticles can be seen along the pore walls of the PAA anodised layer (Fig. 6(b)). The diameters of these nanoparticles correspond with the BC TEOS particles as measured by dynamic light scattering. This indicates that the ingress of the BC TEOS nanoparticles is highly restricted and that formation of a sol–gel network was not possible due to the limited number and spatial separation of the colloids.

3.4. Corrosion resistance

3.4.1. Sulphuric acid anodising

The Bode plot at 0 h for the unsealed and sol–gel sealed SAA layers can be seen in Fig. 7. The unsealed SAA exhibits the characteristic two time constant electrochemical response representative of a hydration sealed porous layer and a barrier layer [31,34]. Both the AC and BC TEOS showed a similar two time constant response however for both systems the impedance values across all frequencies are lower than the SAA unsealed. This suggests that the natural hydration of the SAA layers is inhibited due to the presence of the sol–gels and that protection properties provided by the TEOS sol–gels are inferior to natural hydration. For these systems the low frequency time constant is representative of the barrier layer with the slight reduction in impedance due to the absence of hydration of the barrier layer [33]. The high frequency time constant (~10^4 Hz) for the TEOS sol–gel sealers is likely due to the pore blocking effect of the sealers, or initial hydration occurring to a lesser extent than the SAA blank. The AC and BC PhTEOS sol–gel sealed anodic layers exhibited a phase plot consisting of one time constant only at 0 h. Such a response is typical of barrier oxide films rather than the duplex structure (pore sealant and barrier layer) expected [33,34]. A similar response has also been recorded for electrolytically coloured anodised aluminium where tin is deposited at the base of the pores [32]. The enhanced barrier properties of the organically modified silanes are evident in the elevated impedance values compared to the purely inorganic TEOS. Both the PhTEOS sol–gel sealers exhibited higher impedance than the unsealed SAA, particularly in the low frequency region (<10^2 Hz).

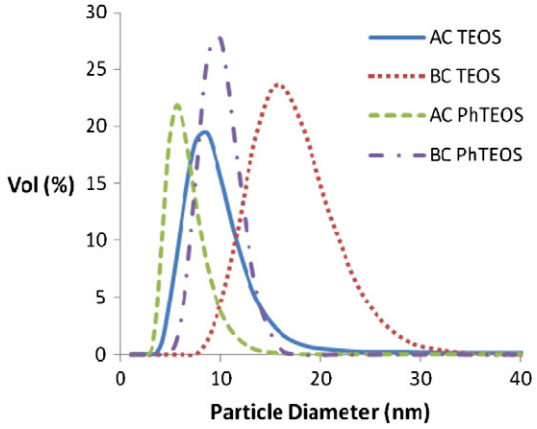

Fig. 2. Particle size distribution of sol–gel sealers.

In order to determine the physical significance of the impedance response equivalent circuit modelling has been conducted using the models in Fig. 8. The model uses the simplified circuit for anodic layer fitting proposed by Hitzig [35], where the pore and barrier layer cells are arranged in series (Fig. 8(a)). This model was used for the unsealed SAA while the sol–gel sealed layers were modelled using the circuit in Fig. 8(b). In this circuit the barrier layer resistance is excluded due to its large contribution or because the porous and barrier layer resistances could not be distinguished. The models include the elements R_s — solution resistance, R_{po} — porous oxide resistance, C_{po} — porous oxide capacitance, R_{bl} — barrier layer resistance and C_{bl} — barrier layer capacitance.

These models were used to fit the recorded EIS spectra for each sealer up to 1000 h exposure and the porous layer resistance values are plotted in Fig. 9. The auto-sealing ability of the unsealed SAA layer was recorded as a small but gradual increase in R_{po} value up to 500 h exposure. Both TEOS sealers appear to have reduced R_{po} values when compared to the unsealed SAA with the PhTEOS based sol–gels providing better pore resistance than the SAA benchmark. Comparing the AC and BC sol–gel equivalent it is noticeable that the BC systems appear to provide a higher level of natural hydration evident from the increase in R_{po} over time. In contrast the AC sol–gels show a decrease in R_{po} up to 336 h before any auto-sealing appears to occur. This suggests that the AC sol–gels, which exhibit better pore impregnation properties, postpone the auto-sealing feature of the SAA anodised films. This postponement allows penetration of the electrolyte into the anodic layer either though the sol–gel matrix or voids between the sol–gel and pore walls. As a result the AC sol–gel systems, which have comparable 0 h R_{po} values to their BC equivalents, experience an initial drop in resistance. Auto-sealing recovery of the anodic film integrity to the initial resistance values requires exposure of up to 1000 h.

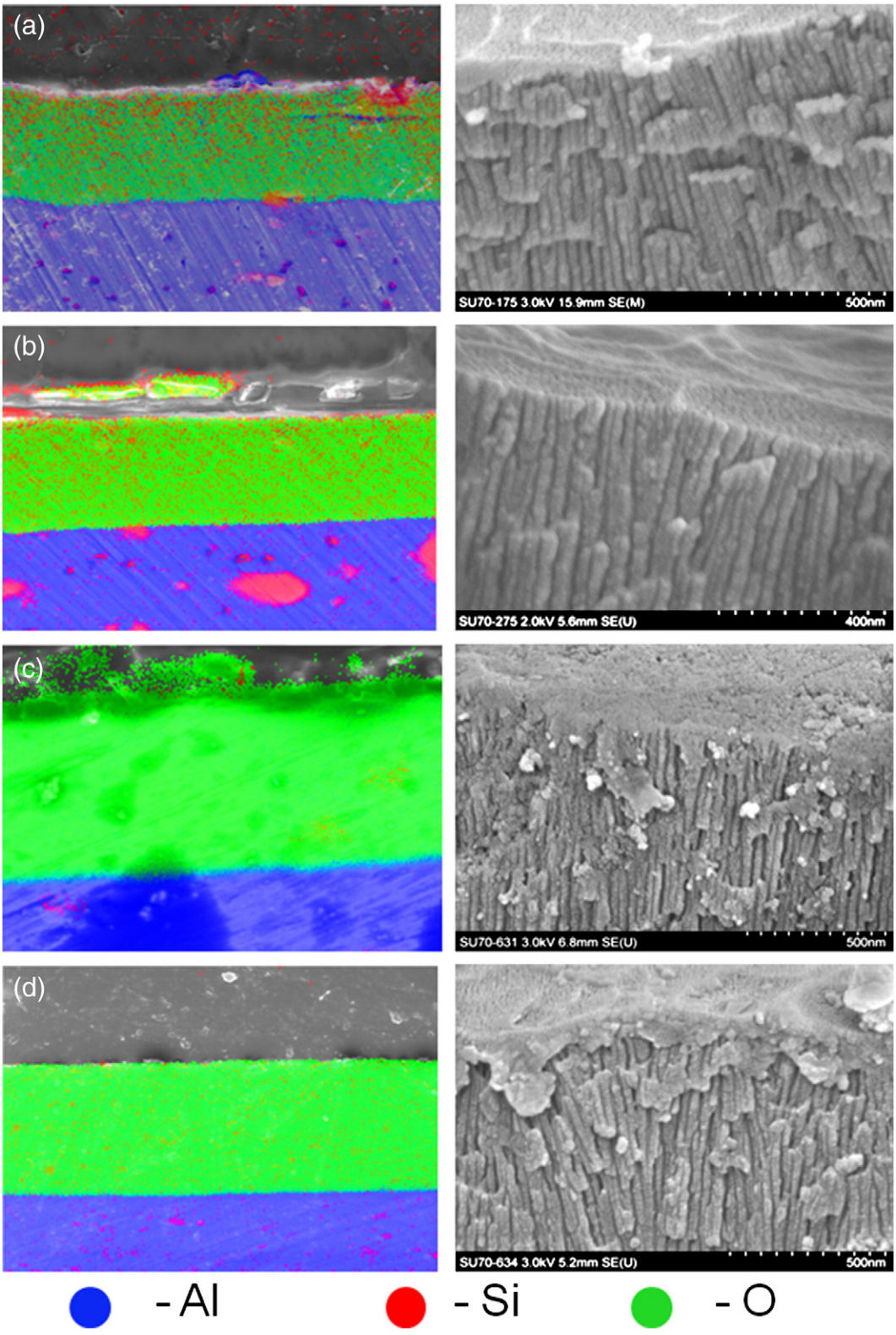

Fig. 3. (Left) — Mixed elemental Dot-Map for SAA sealed films (right) — corresponding to FESEM image (a) AC TEOS, (b) AC PhTEOS, (c) BC TEOS and (d) BC PhTEOS.

Table 2
Sol gel sealing ratings.

Treatments	AC TEOS	AC PhTEOS	BC TEOS	BC PhTEOS
SAA	A3	A3	D3	A3
OAA	A2	A2	D3	C3
PAA	B1	A1	D1	C3

The effect of postponement of hydration on the barrier properties of the anodic layer can be evaluated from the plot of Log |Z| at 0.1 Hz up to 5000 h in Fig. 10. The AC sol–gels and BC PhTEOS exhibit good stability up to 3500 h exposure in the NaCl electrolyte after which the impedance values drop significantly. The AC PhTEOS exhibits a rapid drop initially up to 336 h. After this time the impedance values begin to increase which corresponds with the initiation of auto-

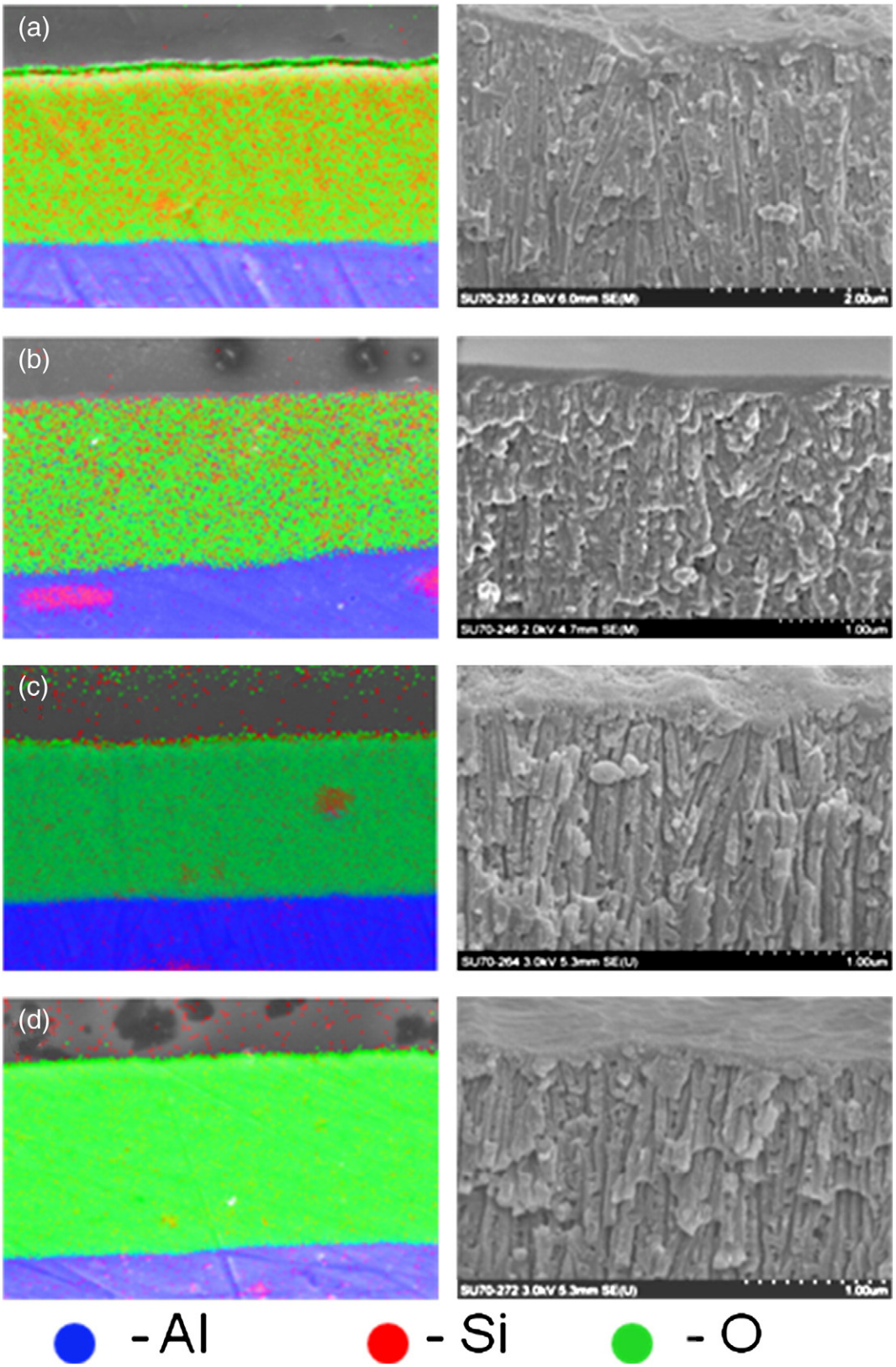

Fig. 4. (Left) — Mixed elemental Dot-Map for OAA sealed films (right) — corresponding to FESEM image (a) AC TEOS, (b) AC PhTEOS, (c) BC TEOS and (d) BC PhTEOS.

sealing from Fig. 9. After 1000 h the impedance values have almost recovered to the 0 h value. At 3500 h exposure the BC PhTEOS exhibits superior barrier properties compared to the other sol–gel treatments and the SAA unsealed.

The long term exposure resistance of sulphuric acid anodised layers has been previously reported and exhibits excellent retention of barrier properties in corrosive environments for up to 25 years [36,37]. The accelerated testing results (Table 3) show that no corrosion developed

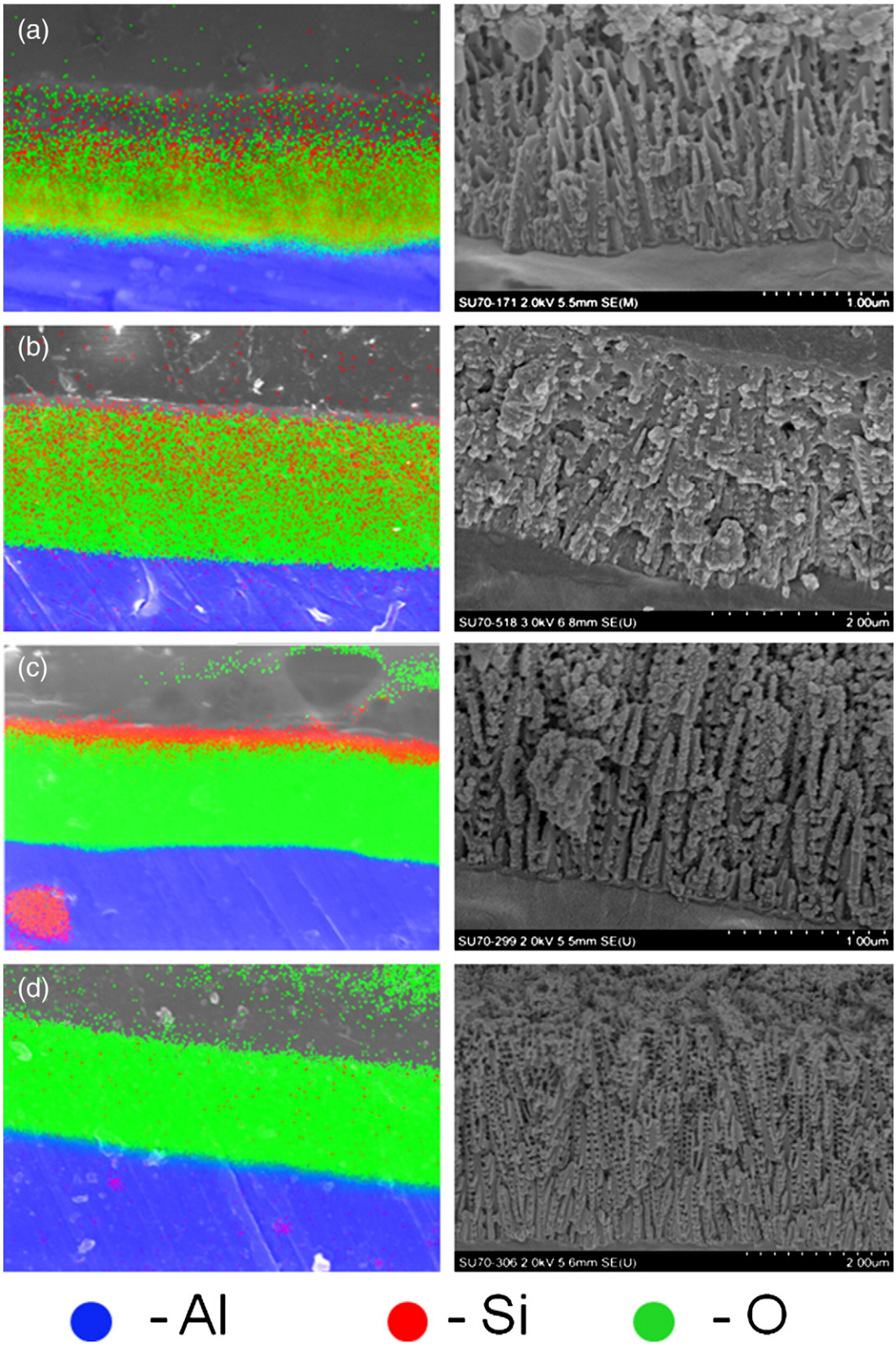

Fig. 5. (Left) — Mixed elemental dot-map for PAA sealed films (right) — corresponding to FESEM image (a) AC TEOS, (b) AC PhTEOS, (c) BC TEOS and (d) BC PhTEOS.

during 2000 h exposure to the NSS environment. This indicates that the natural anticorrosive properties of the SAA layers are retained even with the inclusion of the sol–gel sealers and that any auto-sealing delay is not significant to induce corrosion to the base metal.

3.4.2. Oxalic acid anodising

The Bode plot for the sol–gel sealed OAA layers can be seen in Fig. 11 at 0 h immersion in the 3.5% NaCl solution. The unsealed OAA shows evidence of a duplex sealed structure with a pore and

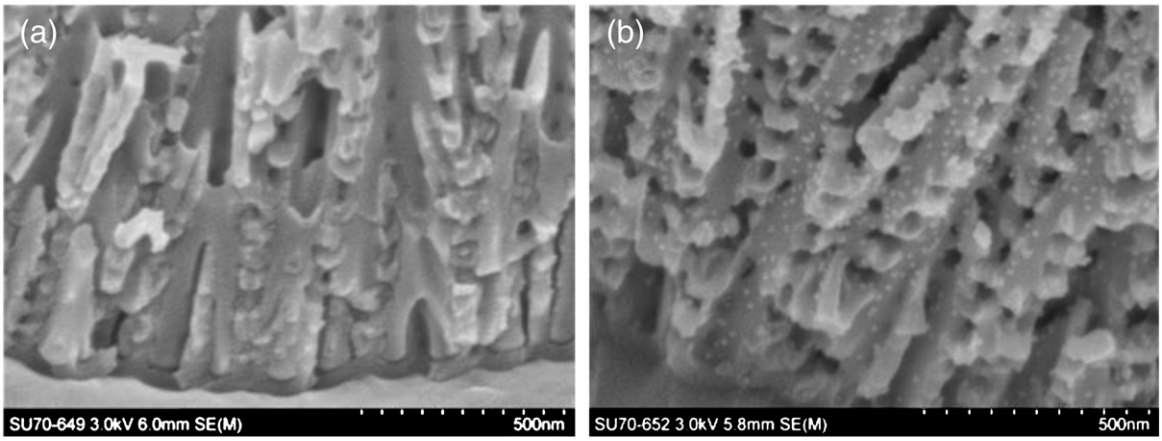

Fig. 6. PAA films with (a) AC-TEOS sol gel filled pores and (b) BC-TEOS nanoparticles on pore walls.

barrier layer response recorded. This suggests that natural hydration has resulted in a closure of the pores. All the sol–gel sealers exhibited a single time constant response which may indicate that the porous layer sealing was inhibited by the sol–gel treatment or that the electrochemical response from the sol–gel and barrier layer could not be distinguished. The AC PhTEOS appears to have increased barrier properties when compared to the OAA unsealed. The remaining sol–gel treatments showed inferior high frequency impedance when compared to the unsealed OAA with the BC PhTEOS showing better sealing properties compared to the purely inorganic TEOS sealers. Fig. 12 displays the Bode plots after 2000 h exposure for the sealing systems. After this time the AC PhTEOS retains excellent stability compared to the other sol–gel systems and the unsealed OAA, all of which exhibit an impedance modulus drop of at least 2 orders of magnitude from 0 h. Three time constants are recorded for the unsealed OAA with the third appearing due to the onset of corrosion. The remaining systems (AC and BC TEOS and BC PhTEOS) all exhibit inferior impedance values compared to the unsealed OAA after 2000 h exposure.

From Fig. 13 it can be seen that the AC sealers exhibit superior low frequency impedance stability than the BC equivalents. This is possibly due to the increased impregnation and pore filling capability of the AC systems as measured by FESEM and EDX. Interestingly, the BC systems experienced a rapid drop in protection properties compared to the unsealed OAA suggesting that the natural hydration of the OAA layers is compromised by the presence of the BC sol–gel treatments. The BC TEOS system, in particular, caused a severe decline in protection properties with corrosion evident after only 48 h exposure to the NaCl solution. Such deterioration in corrosion resistance over the unsealed OAA sample suggests that the BC systems are not appropriate for sealing of OAA surfaces.

The EIS and NSS testing results are in good agreement with the unsealed OAA free from pitting for the duration of the test (Table 3). Also recorded from the EIS analysis, the AC and BC TEOS and BC PhTEOS films had a negative effect on the performance of the OAA with pitting occurring within 24 h exposure. This also indicates some influence on the hydration process of the OAA surface as the protection of the OAA blank can only be attributed to the extent that the pores have sealed naturally. The applied sealers appear to have inhibited this self sealing while the protection provided by the sol–gel material is not sufficient to prevent pitting. The AC PTEOS showed equivalent pitting resistance to the OAA blank up to 2000 h.

3.4.3. Phosphoric acid anodising

Due to the absence of self hydration the impedance spectra from PAA films are comprised of one time constant due the response from the barrier layer oxide only, Fig. 14. The recorded unsealed PAA EIS spectrum is similar to that of bare 3003 aluminium suggesting the PAA treatment alone provides little protection to the aluminium. This indicates that the integrity of the barrier layer is easily compromised upon exposure to the electrolyte. All of the sol–gel treated PAA layers exhibited one time constant. Furthermore all the sol–gel treatments had a positive influence on the low frequency impedance values indicating that sealing was enhanced by the inclusion of the sol–gel treatment. The PhTEOS based sealers again exhibited superior properties in sealing the anodised layers with the AC PhTEOS increasing impedance values across the entire frequency range. This is expected due to the

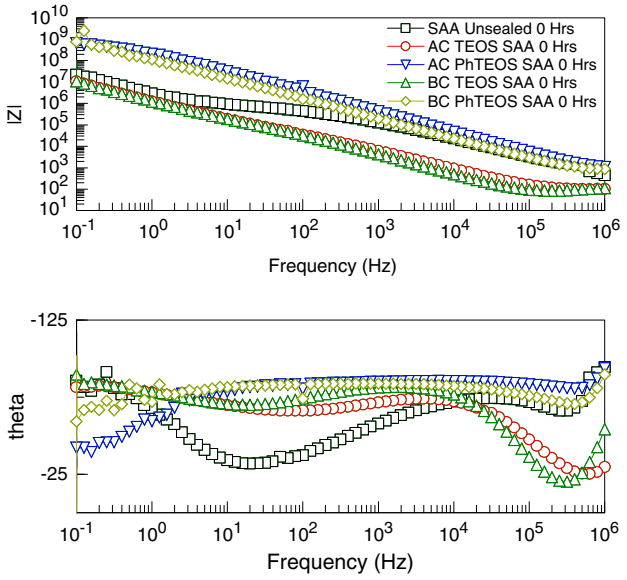

Fig. 7. 0 h Bode plots showing (top) the impedance and (bottom) the phase angle for SAA sol–gel sealed anodic films.

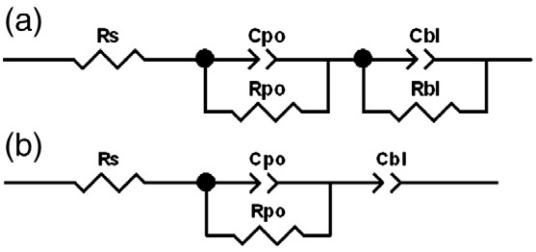

Fig. 8. Data fitting equivalent circuits (a) simplified model for sealed anodised aluminium (b) with barrier layer resistance removed.

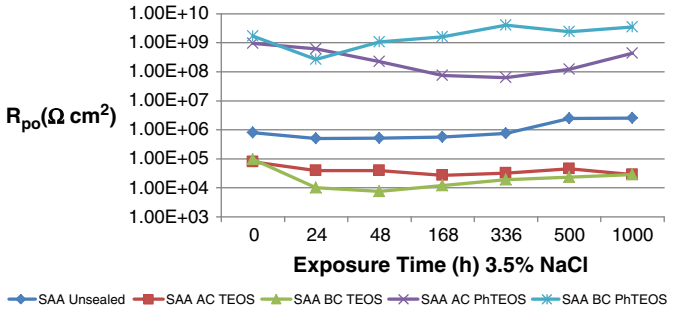

Fig. 9. R_{po} evolution over time for SAA sol gel sealers.

high level of sealing detected by SEM and EDX analyses. From the Log |Z| at 0.1 Hz plot, Fig. 15, it is seen that all the sol–gel sealed layers exhibited significant degradation of barrier properties after relatively short immersion times with the AC PhTEOS retaining the highest impedance values during the exposure duration. After 24 h exposure the BC TEOS samples exhibited a response similar to the PAA unsealed. As this system exhibited a surface film only from the FESEM and EDX analyses it is possible that once this film is compromised, and the electrolyte penetration occurs, the response reverts to that of unsealed PAA.

In NSS the worst performing treatments are the PAA films perhaps due to the large pore size and lack of self sealing properties (Table 3). It is seen that the AC and BC TEOS films caused little improvement in the corrosion performance where other hydration effects do not affect the surface properties. The best treatment on the PAA surface is AC PTEOS with no pitting occurring up to 500 h.

4. Discussion

Investigations into the combination of sol–gel chemistries as sealing agents for anodised aluminium are limited to date. This study investigated the effect of pore size and colloid properties on the synergistic combination of sol–gels and anodisation. This initial study has found that:

1) Sol–gel materials can be impregnated into the pores of anodic layers without the influence of an electromotive force or vacuum deposition.
2) The sol–gel colloid size has only a limited effect on the penetration and sealing of the oxide layers with anodising electrolyte type and sol–gel pH having a greater influence.
3) The sol–gel materials can enhance the protection provided by anodised films however certain formulations appear to affect the natural corrosion resistance mechanisms of anodic films.

There are numerous factors that may influence the possibility of migration and encapsulation of particulate materials in porous membranes such as relative diameter between particles and pores, surface charge between pore walls and liquid, surface tension of the liquids

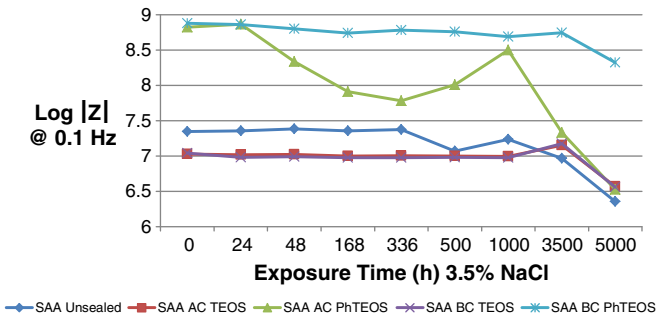

Fig. 10. Log |Z| at 0.1 Hz for SAA sol–gel sealers.

Table 3
Pitting rating for sol gel sealed anodised aluminium surfaces.

Sample	First sign of corrosion (h)	Corrosion rating @ 2000 h
SAA Blank	–	0
SAA AC TEOS	–	0
SAA AC PhTEOS	–	0
SAA BC TEOS	–	0
SAA BC PhTEOS	–	0
OAA Blank	–	0
OAA AC TEOS	24	1
OAA AC PhTEOS	–	0
OAA BC TEOS	24	6
OAA BC PhTEOS	96	3
PAA Blank	24	50
PAA AC TEOS	24	50
PAA AC PhTEOS	500	50
PAA BC TEOS	24	50
PAA BC PhTEOS	168	50

and chemical alteration or attack of the pore walls by the impinging liquid. It is likely that a combination of these factors determines the probability of sol–gel penetration and sealing of anodic layers.

In relation to relative diameters, it can be seen that the ratio of pore size to sol–gel particle diameter has a minimal effect on penetration into the oxide layers. Penetration will not occur unless the particle size is sufficiently small to enter the pores although this does not seem to be the only determining factor. It has been shown previously that particle size is significant for nanoparticle incorporation in anodic films with trace amounts of both positively and negatively charged nanoparticles penetrating porous aluminium oxide films [28]. For the base catalysed systems it is evident that sol–gel penetration is significantly less than for the corresponding acid catalysed systems. Only the BC PhTEOS sealed SAA achieved an A penetration rating with all other BC systems exhibiting ratings of C or D. Both the base catalysed systems had slightly larger colloid diameters than the AC equivalents. This particle size is below the diameters of the OAA and PAA pores. In both cases limited sealing occurred inferring that other effects are responsible for the restricted penetration into the oxides. Interestingly surface films (D ratings) occurred for BC TEOS sol–gels only indicating that the viscosity or surface tension is unique from the other chemistries used for sealing resulting in surface films rather than pore sealers. Surface tension in particular has been shown to be an important effect for

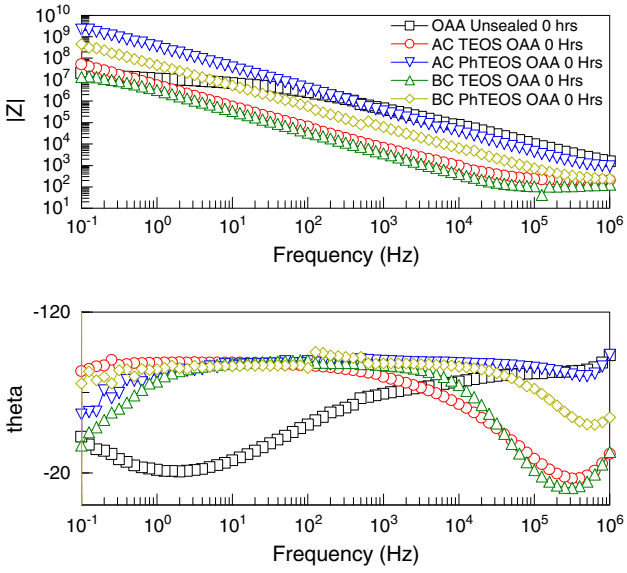

Fig. 11. 0 h Bode plots showing (top) the impedance and (bottom) the phase angle for OAA sol–gel sealed anodic films.

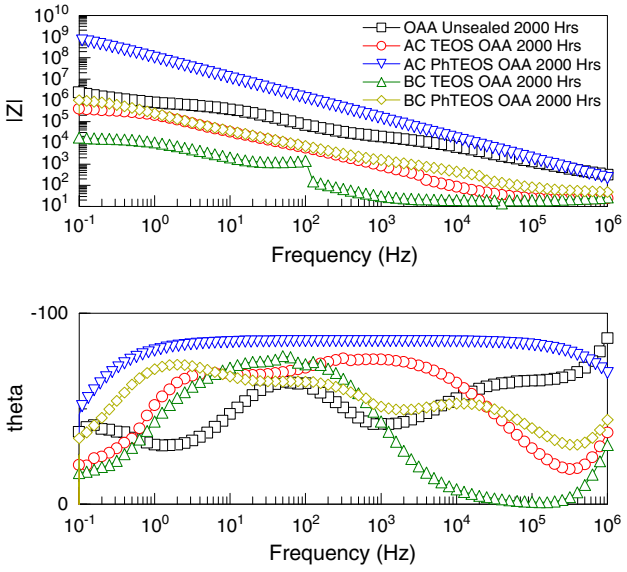

Fig. 12. 2000 h Bode plots showing (top) the impedance and (bottom) the phase angle for OAA sol–gel sealed anodic films.

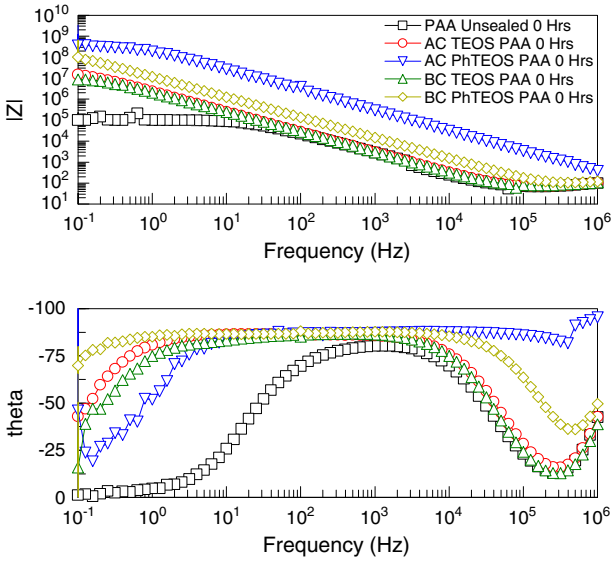

Fig. 14. 0 h Bode plots showing (top) the impedance and (bottom) the phase angle for PAA sol–gel sealed anodic films.

solvent filling of porous anodic alumina [38]. The wetting and penetration of solvents on porous anodic alumina has been shown to be strongly dependent on the polar nature of the solvents used with inherent difficulties experienced with aqueous based solutions. It is also proposed that liquids may wet the pore walls only. If the adhesive force of the liquid on the pore walls is strong enough to overcome the cohesive force of the liquid then pores will be filled with the solution, if not the penetration of liquid into the pores will be slow with several months or years required for full pore filling.

For sol–gel impregnation of oxide layers surface charge may also be very significant as conventionally sealing solutions and dyes require close pH monitoring to achieve full pore penetration [1]. This feature may apply to the current study especially if there is no significant chemical interaction between the sol–gel and the oxide surface. The colloidal sol–gel solutions used have varying surface charges depending on the pH and the functionality of the silane precursors used. It has been shown that the isoelectric point and surface charges will change by altering the chemistry of a silica surface by changing the functionality of the silane precursor [39]. Therefore the differences in surface charge between acid and base catalysed systems caused by the pH of the sol–gel and functionality of the silane monomers may be responsible for the significant differences in sol–gel penetration into the oxide layers.

It is reported that the pore walls of anodic alumina formed in various electrolytes retain some anions of the electrolyte (sulphates, oxalates, phosphates) adsorbed on the pore wall surface which are subsequently replaced by OH^- during hot water sealing [40]. This ion exchange mechanism has been used to explain hydrothermal sealing and may possibly be applied to sol–gel sealing. Under acidic conditions condensed species are expected to have neutral charge while partial condensation of silanes in alkaline conditions results in ionised species [14] which may be more reactive with the pore walls of the anodic alumina. Base catalysed sol–gel colloids are charged by surface coverage of OH^- which can participate in ion exchange with anions from the electrolyte in which the film was formed. The effect of this would be more surface specific sealing for base catalysed sol–gel systems, blocking the pore mouth and preventing full penetration of the sol–gel. This feature is confirmed for the BC TEOS on all surfaces and the BC PhTEOS on the OAA and PAA films. There may also be a chemical dissolution effect of the basic high pH of the BC systems on the aluminium oxide influencing this feature.

By assigning the ratings it is evident that there is a similarity in the sol–gel penetration on all anodising finishes with better pore sealing occurring with the larger pore diameter systems. The OAA and PAA treatments appear to be better host matrices than the SAA anodic layers particularly for AC sol gels. The possibility of hydration of the OAA pores limits their use while the open structure of the PAA layers may be convenient where controlled film thickness and hosting ability are required. The PAA substrate, which exhibited interporosity, acts as an excellent host matrix for the AC sol–gel systems. This interporosity dispels any pressure build up in the pores of the anodised layer as a result of the increasing confinement by the impinging liquid.

From the corrosion resistance testing, by both electrochemical and accelerated exposure, it is evident that the combination of anodising process and sol–gel must be chosen carefully to prevent deterioration

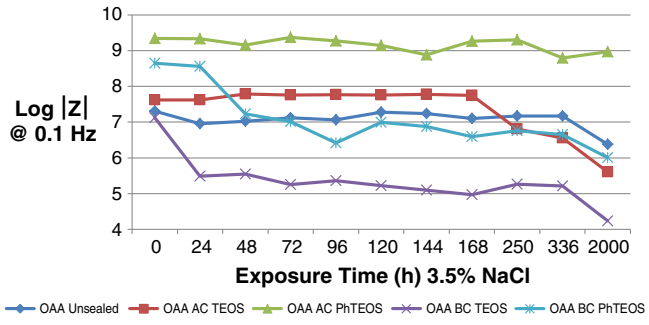

Fig. 13. Log |Z| at 0.1 Hz for OAA sol–gel sealers.

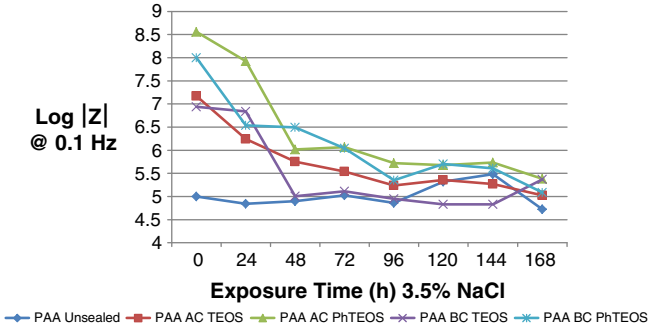

Fig. 15. Log |Z| at 0.1 Hz for PAA sol–gel sealers.

of the natural sealing properties of anodised layers. The negative effect on the OAA layers is significant and indicates that care should be taken if natural hydration of oxide layers is adversely influenced by any posttreatment. The postponement of the auto-sealing of the SAA layers is evident from the EIS data fitting for the AC systems however the salt spray performance of all the SAA sol–gel treated samples suggests that this delay in auto-sealing is not damaging to the long term corrosion resistance of the anodic layers. The corrosion resistance of the PAA layers can be improved with the addition of a sol–gel sealing agent. PAA is not a conventional treatment for corrosion protection however with correct encapsulation of sol–gel an acceptable level of corrosion resistance can be achieved.

5. Conclusion

The penetration properties of the sol–gel materials appeared independent of the pore sizes of the anodic surface treatments. Acid catalysed sol gel systems have a higher affinity for pore penetration with a high level of pore filling achieved for relatively short immersion times. It is shown that the resulting corrosion resistance properties are significantly affected by the initial anodising process with evidence that some sol gel sealers can have an adverse effect on the hydration of the oxide surfaces. In general the acid catalysed sol–gel systems provide superior corrosion resistance compared to the equivalent base catalysed silanes. Sol–gel sealers prepared from organically modified silanes showed significantly better corrosion performance compared to purely inorganic systems.

Acknowledgements

This work is supported by the European Union under the Seventh Framework Programme, project 266029 “Aeromuco”.

References

[1] S. Wernick, R. Pinner, P.G. Sheasby, The surface treatment and finishing of aluminum and its alloys, 5th ed., Finishing Publications Ltd., 1987
[2] V.F. Henley, Anodic Oxidation of Aluminium & Its Alloys, Pergamon Press, 1982.
[3] S.J. Garcia-Vergara, L. Iglesias-Rubianes, C.E. Blanco-Pinzon, P. Skeldon, G.E. Thompson, P. Campestrini, Proc. R. Soc. A Math. Phys. Eng. Sci. 462 (2006) 2345–2358.
[4] S.J. Garcia-Vergara, P. Skeldon, G.E. Thompson, H. Habazaki, Corros. Sci. 49 (2007) 3772–3782.
[5] S.J. Garcia-Vergara, P. Skeldon, G.E. Thompson, T. Hashimoto, H. Habazaki, J. Electrochem. Soc. 154 (2007) C540–C545.
[6] S.J. Garcia-Vergara, P. Skeldon, G.E. Thompson, H. Habakaki, Appl. Surf. Sci. 254 (2007) 1534–1542.
[7] J. Zhao, L. Xia, A. Sehgal, D. Lu, R.L. McCreery, G.S. Frankel, Surf. Coat. Technol. 140 (2001) 51–57.
[8] F. Snogan, C. Blanc, G. Mankowski, N. Pebere, Surf. Coat. Technol. 154 (2002) 94–103.
[9] R.B. Mason, S. Clark, M. Klingenberg, E. Berman, N. Voevodin, Met. Finish. 104 (2011) 4–5.
[10] P.C.R. Varma, J. Colreavy, J. Cassidy, M. Oubaha, B. Duffy, C. McDonagh, Prog. Org. Coat. 66 (2009) 406–411.
[11] P.C.R. Varma, P. Periyat, M. Oubaha, C. McDonagh, B. Duffy, Surf. Coat. Technol. 205 (2011) 3992–3998.
[12] R.V. Padinchare Covilakath, J. Cassidy, M. Oubaha, C. McDonagh, J. Colreavy, B. Duffy, ECS Trans. 24 (2010) 231–246.
[13] J. Livage, M. Henry, C. Sanchez, Prog. Solid State Chem. 18 (1988) 259–341.
[14] G.S.C.J. Brinker, Sol–Gel Science: The Physics and Chemistry of Sol–Gel Processing, Academic Press, San Diego, CA, 1990.
[15] L.L. Hench, J.K. West, Chem. Rev. 90 (1990) 33–72.
[16] C.J. Brinker, G.C. Frye, A.J. Hurd, C.S. Ashley, Thin Solid Films 201 (1991) 97–108.
[17] M.L. Zheludkevich, I.M. Salvado, M.G.S. Ferreira, J. Mater. Chem. 15 (2005) 5099–5111.
[18] M. Guglielmi, J. Sol–Gel Sci. Technol. 8 (1997) 443–449.
[19] C. Sanchez, B. Julian, P. Belleville, M. Popall, J. Mater. Chem. 15 (2005) 3559–3592.
[20] P. Gomez-Romero, C. Sanchez, Functional Hybrid Materials, Wiley-VCH, Weinheim, 2004.
[21] R.L. Parkhill, E.T. Knobbe, M.S. Donley, Prog. Org. Coat. 41 (2001) 261–265.
[22] S. Hirai, K. Shimakage, S. Aizawa, K. Wada, J. Am. Ceram. Soc. 81 (1998) 3087–3092.
[23] S. Hirai, K. Shimakage, M. Sekiguchi, K. Wada, A. Nukui, J. Am. Ceram. Soc. 82 (1999) 2011–2015.
[24] L.Y.L. Wu, S. Nemeth, MRS Proc. 778 (2003) U8.7/W7.7.
[25] T. Liu, F. Zhang, C. Xue, L. Li, Y. Yin, Surf. Coat. Technol. 205 (2010) 2335–2339.
[26] D. Xu, Y. Yu, M. Zheng, G. Guo, Y. Tang, Electrochem. Commun. 5 (2003) 673–676.
[27] Z. Miao, D. Xu, J. Ouyang, G. Guo, X. Zhao, Y. Tang, Nano Lett. 2 (2002) 717–720.
[28] K. Kai, F. Haruto, M. Keita, Y. Yukiko, N. Masumi, H. Shunji, M. Yasumichi, Electrochem. Solid-State Lett. 7 (2004) B25–B28.
[29] G. Boisier, N. Pébère, C. Druez, M. Villatte, S. Suel, J. Electrochem. Soc. 155 (2008) C521–C529.
[30] J.J. Suay, E. Gimenez, T. Rodriguez, K. Habbib, J.J. Saura, Corros. Sci. 45 (2003) 611–624.
[31] L. Domingues, J.C.S. Fernandes, M. Da Cunha Belo, M.G.S. Ferreira, L. Guerra-Rosa, Corros. Sci. 45 (2003) 149–160.
[32] M. Franco, S. Anoop, R. Uma Rani, A.K. Sharma, ISRN Corros. 12 (2012), [2012 Article ID 323676].
[33] M. García-Rubio, M.P. de Lara, P. Ocón, S. Diekhoff, M. Beneke, A. Lavía, I. García, Electrochim. Acta 54 (2009) 4789–4800.
[34] M. Whelan, K. Barton, J. Cassidy, J. Colreavy, B. Duffy, Surf. Coat. Technol. 227 (2013) 75–83.
[35] J. Hitzig, K. Jüttner, W.J. Lorenz, W. Paatsch, J. Electrochem. Soc. 133 (1986) 887–892.
[36] M.J. Bartolomé, J.F. del Río, E. Escudero, S. Feliu Jr., V. López, E. Otero, J.A. González, Surf. Coat. Technol. 202 (2008) 2783–2793.
[37] E. Escudero, V. López, E. Otero, M.J. Bartolomé, J.A. González, Surf. Coat. Technol. 201 (2007) 7303–7309.
[38] R. Redón, A. Vázquez-Olmos, M.E. Mata-Zamora, A. Ordóñez-Medrano, F. Rivera-Torres, J.M. Saniger, J. Colloid Interface Sci. 287 (2005) 664–670.
[39] K. Hasegawa, S. Kunugi, M. Tatsumisago, T. Minami, J. Sol–Gel Sci. Technol. 15 (1999) 243–249.
[40] J.W. Diggle, T.C. Downie, C.W. Goulding, Chem. Rev. 69 (1969) 365–405.